Applied Solid Mechanics coursework assessment

Darian Irani

PART A: FEA investigation and report

PROBLEM OUTLINE

The following report presents a 'proof-of-concept design' on a lifting lug of a Gas Combustion Unit (GCU), conducting an analysis on the deflection and stress of the lug during its operation. The aim of this stress analysis report is to determine whether six lugs attached to the GCU are designed well enough to keep the GCU safe and stable while it is lifted and to determine whether the lugs will experience any yielding or fracture. The deflection and stress of the lug is modelled numerically using Abaqus CAE [1] software and validated to ensure that the calculated results are accurate and realistic.

MATERIAL PROPERTIES, LOADING, AND GEOMETRY

The stress analysis of the lugs lifting the GCU uses the following assumptions and hence is not considered as a factor that impacts any of the analysis. Firstly, it is assumed that the structural integrity of the weld connecting the lug and the GCU is sufficient for the operation and does not affect the stress of the lug. Secondly, it is assumed that the GCU is lifted in ambient environmental conditions and hence factors such as heavy wind or intense weather is not accounted for in the stress analysis. Lastly, it is assumed that the GCU is lifted at constant velocity and hence the gravitational acceleration remains constant.
Abaqus CAE software is used to simulate the load experienced per lug and numerically calculate the lug's stress and deflection. Figure 1(d) shows the Abaqus CAE lug assembled with a shackle and a pin. Figure 1(a), (b), and (c) show the geometry of the lug and its shackle. The load experienced by each of the six lugs attached to the GCU is calculated using equation 1 and ultimately gives a value of 58,860N. Table 1 shows the material properties of the chosen lifting lug material – Steel (EN10025-2- S355JR).

$$F = \frac{mg}{6} \tag{1}$$

where, m is the overall mass of the GCU (kg) and g is gravitational acceleration (ms^{-2})

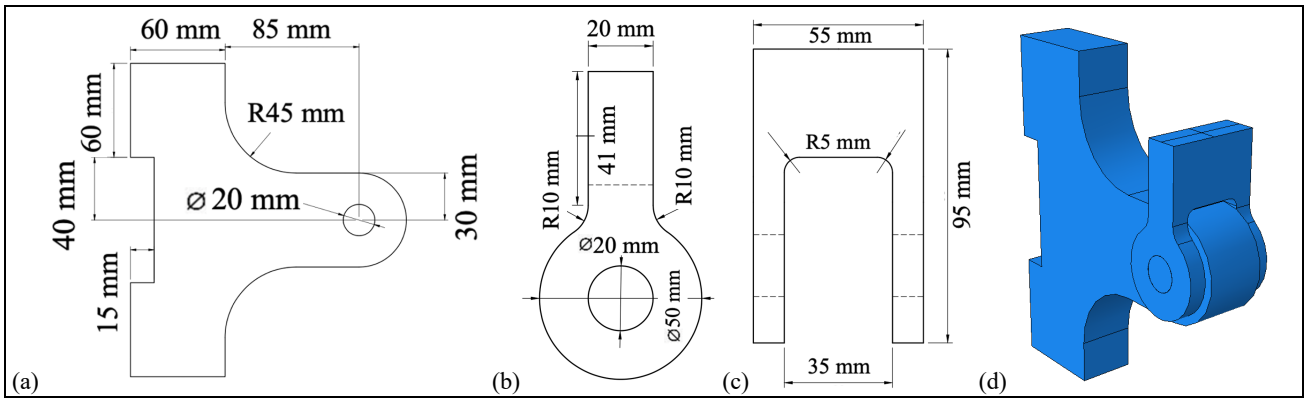

Fig. 1 Displays a geometry of (a) lifting lug where the uniform thickness is 35 mm, geometry of (b) side view of shackle and (c) front view of shackle, (d) Abaqus CAE model of the lug assembled with a pin and shackle.

Table 1: Ambient-temperature mechanical properties of structural steel used for the lifting lugs (Steel, EN 10025-2 – S355JR) [2].

Property	Value
Young's Modulus	209 GPa
Poisson's Ratio	0.3
Yield Strength	355 MPa
Ultimate tensile strength (UTS)	630 MPa
Elongation at failure	22%
Density	8010 kgm^{-3}

FINITE ELEMENT (FE) ANALYSIS

Setting Abaqus CAE inputs

Firstly, the lug's material properties in Table 1 and boundary conditions are added onto the model on Abaqus CAE. The surfaces that connect the lug to the GCU through welding are fixed and is therefore constrained in all directions. A shackle and a pin are designed to fit onto the lug, as seen in Figure 1(d), the purpose of this addition is to simulate the load and stress more accurately. The addition of a shackle simulates the tensile load of the GCU more realistically because in a real-life scenario the lug would ideally be assembled with a pin and shackle. As a result, a concentrated load is added on the Abaqus CAE model which acts on the upper surface of the shackle to simulate the tensile load experienced by the lug through a connected instrumentation cable. The pin is assumed to be fitted with an interference fit into the hole of the lug and therefore there is no spacing between the hole and the pin. An interaction is added on Abaqus CAE to model the friction between the pin and the shackle, this provides the model with a more accurate calculation of stress at the contact region because friction between the parts would increase the stress in the lug [3].

Regarding the meshing technique of the lug, a hexahedral mesh type is chosen over the tetrahedral type as it provides a more accurate solution, this is because the hexahedral mesh type increases the node density along curved regions to capture flows along that surface accurately [4]. Since the Abaqus CAE assembly has three different parts, an independent part instance is used on the lug, pin, and shackle as a more refined mesh is aimed to be used on the lug part. Next, a quadratic element type is used over a linear element type as a quadratic choice utilizes a non-linear shape function and the displacements between the nodes are interpolated using a higher order polynomial. Quadratic elements are better suited to this analysis of the lug as it is better suited to accurately represent complex geometries and bending deformations of the part [5]. Lastly, regarding the element size chosen for the FE analysis, a default element size of 50 is initially chosen and the tip deflection is recorded, the tip deflection at half the first element size (size 25) is then recorded and the error is calculated using equation 2. The same process is repeated until there is a negligible error in the first and second deflection values. This process resulted in a element size of 6 to be used for the FE analysis.

$$E = \frac{|\delta_2 - \delta_1|}{|\delta_2|} \tag{2}$$

where, E is the error, δ_2 is the tip deflection value at the bigger element size, and δ_1 is the tip deflection value at the first element size divided by two.

Numerical results

Figure 2 shows a contour of how the maximum deflection and maximum non-contact Von Mises stress varies on different parts of the lug assembly.

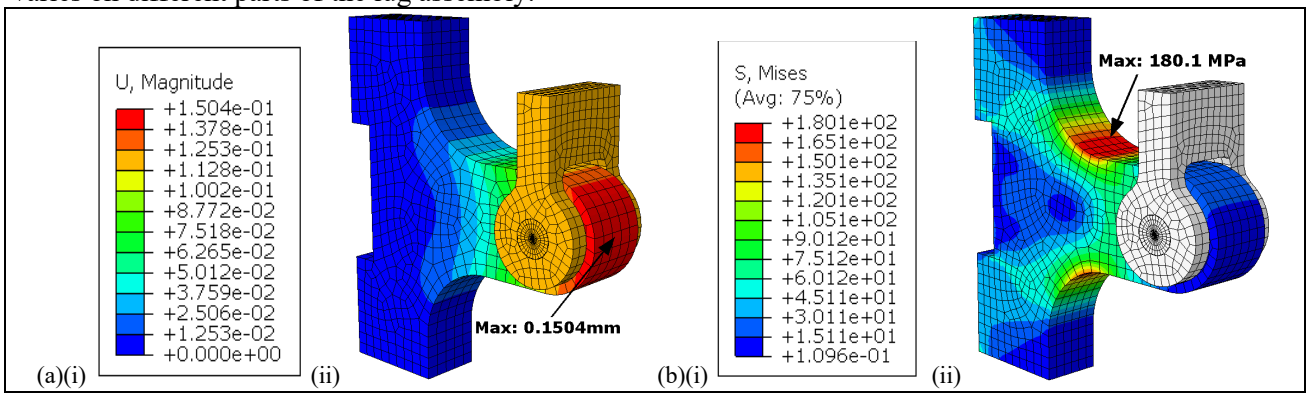

(a)(i) (ii) (b)(i) (ii)

Fig. 2 Displays a contour of how the (a) vertical deflection and (b) Von Mises stress varies on different sections of the lug assembly.

The maximum vertical deflection at the end of the lifting lug is 0.1504mm, the maximum Von Mises stress excluding the contact region between the lug and lifting shackle is 180.1 MPa, and the maximum Von Mises stress at the contact region is 217.6 MPa.

FINITE ELEMENT MODEL VALIDATION

Mesh convergence study

A convergence study on the stress and deflection of the lug is conducted to determine what seeding size allows the model's numerical solution to tend towards a unique value. As the mesh density of the Abaqus CAE model increases, if two meshes give a similar result it can conclude that the model is producing a mathematically accurate solution. The study is conducted on the lug's non-contact stress as the contact stress is susceptible to possible non-convergence due to stress singularity. Given that the load is simulated as a 'concentrated load', it is assumed that the force acts on a singular node. As the mesh is refined the area around the node becomes smaller which means the stress always increases and hence never converges [6]. Figure 3 displays how the stress and deflection changes as the mesh density is increased, the mesh is 'converged' when further mesh refinement produces a negligible change in stress and deflection values [7].

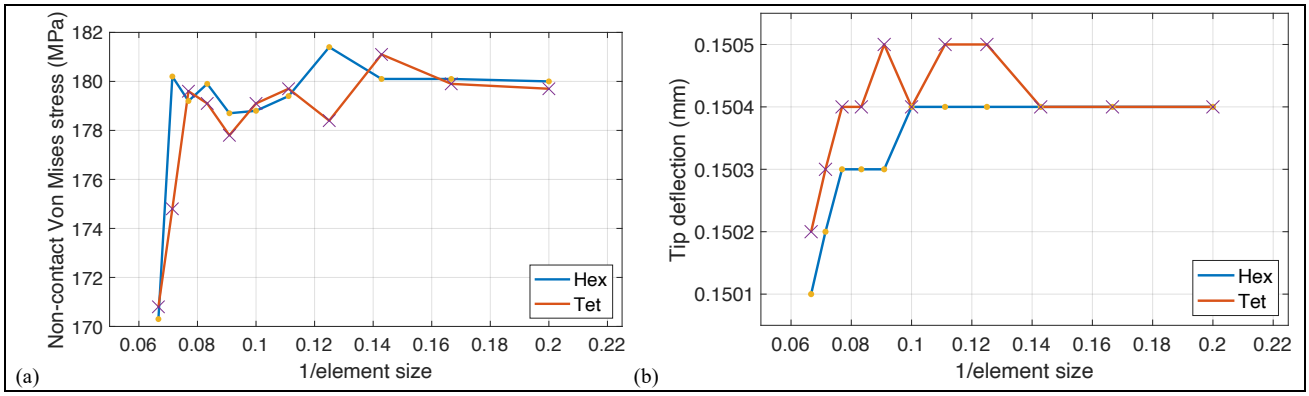

Fig. 3 Convergence plot of (a) non-contact Von Mises stress and (b) tip deflection in the lug using a quadratic hexahedral and tetrahedral mesh.

The mesh convergence study shows that the hexahedral mesh type converges quicker than the tetrahedral type for both stress and deflection, therefore making it the chosen mesh type for the lug's FE analysis.

Analytical solution comparison

A validation is conducted to ensure that the Abaqus CAE model considers the physical effects concerning the lug and to ensure the input parameters such as units are correct. The maximum deflection and stress values obtained through the lifting lug FE analysis on Abaqus CAE need to be validated with an analytical solution to justify the integrity of the numerical results. Identical results from an analytical solution and Abaqus CAE calculated values would imply that the FE analysis conducted is valid and can therefore be considered as an accurate presentation of deflection and stress in the lifting lug for its use in lifting the GCU safely.

The analytical solution for maximum vertical deflection of the lug is validated using equation 3, which uses values calculated in equation 4 and 5. For analysing the deflection of the lug, the lug is assumed to be a fixed cantilever beam with constant rectangular cross-sectional area having overall dimensions 35x60x85mm (refer to figure 1a). Hence, equation 3 is a derivation from Timoshenko's beam theory [8] and is deliberately chosen over the Euler-Bernoulli beam theory as it calculates the tip deflection more accurately. The Timoshenko beam theory is better suited for short, thick beams and includes the effects of shear deformation, both these factors ultimately make it the more accurate equation to use for calculating tip deflection. The analytical solution for tip deflection of the lug calculates a value of 0.1271 mm, the Abaqus CAE FE analysis provides a value of 0.1504 mm. These two values result in an error of 18.3%, the slight discrepancy in deflection is due to the existence of the lug hole and chamfered edges. However, the error is not significant enough to invalidate the FE analysis of the lug's tip deflection and therefore the Abaqus CAE numerical solution of the maximum tip deflection is valid.

$$\delta_{tip} = \frac{PL^3}{3EI} + \frac{PL}{\kappa GA} \tag{3}$$

where, P is the tensile load (N), L is the distance labelled '85mm' on Figure 1(a), E is the Young's modulus (MPa) (refer to Table 1), I is the horizontal axis moment of inertia (mm^4), κ is the ratio of displacements for a rectangular cross-sectional area (0.83), G is the shear modulus, A is the cross-sectional area of the lug.

$$I = \frac{bh^3}{12} \tag{4}$$

where, b is the thickness of the lug (mm), h is the distance labelled '30mm' multiplied by two on Figure 1(a).

$$G = \frac{E}{2(1+\upsilon)} \tag{5}$$

where, υ is the Poisson's ratio from Table 1.

The analytical solution for stress acting on the lug is validated by comparing the Abaqus CAE contact stress value with equation 6. The stress validation equation uses concepts from 'Contact Mechanics' to calculate a stress value for the lug. The equation uses the concept of 'Bearing Pressure' which calculates the pressure caused through the contact of a convex surface (the pin) and a concave surface (the lug hole) [9]. Since the lug model is constrained in the x and z direction, only the pressure in the y direction is considered (S_{22} view on Abaqus CAE). The analytical solution for the maximum stress in the lug calculates a value of 107.1 MPa, the Abaqus CAE FE analysis provides a value of 114.7 MPa. These two values result in an error of 7.1%, this can be considered as a negligible error and therefore implies that the Abaqus CAE numerical solution of the stress experienced by the lug is valid.

$$P_{max} = \frac{4}{\pi} \cdot \frac{F}{L \cdot D} \tag{6}$$

where F is the tensile load (N), L is the thickness of the lug (mm), D is the diameter of the lug's hole.

EVALUATION OF DESIGN

In summary, this report analyses the effects of the GCU mass on each of the six lugs attached to it and considers the integrity of its design with relation to how its vertical deflection and stress varies on different sections of the lug part. Prior to the FE analysis, several assumptions are stated to point out factors that could possibly affect the calculated stress and deflection values. Design of the lug's welding, environmental conditions, and the way the lug is lifted are all factors that need to be thoroughly considered to ensure the calculated stress and deflection values are what they would be in a real-life scenario. A strength of the FE analysis of the lug assembly is the addition of a pin and shackle for more accurate load and stress simulation. A possible limitation of the FE analysis is the stress and deflection analytical solution errors, a possible way to mitigate the slight discrepancy is to refine the mesh further for better results.

REFERENCES

[1] *Abaqus CAE - Finite element modeling, visualization, and process automation*. Available at: https://www.3ds.com/products-services/simulia/products/abaqus/abaquscae/

[2] Harry Coules & Alexander Velichko, 07/11/2022, MENG 30011 Applied Solid Mechanics, AY 2022/23 coursework assessment, University of Bristol.

[3] *Abaqus Theory Manual (V6.6)*. Available at: https://classes.engineering.wustl.edu/2009/spring/mase5513/abaqus/docs/v6.6/books/stm/default.htm?startat=ch05s02ath135.html.

[4] https://resources.system-analysis.cadence.com/blog/msa2022-hexahedral-mesh-vs-tetrahedral-comparing-high-quality-meshing

[5] The_Analyst (2022) *Linear vs quadratic FE elements*, *FEA Tips*. Available at: https://featips.com/2019/03/29/linear vs quadratic-fe-elements/.

[6] Ph.D., Ł.S. (2021) *Stress singularity - an honest discussion*, *Enterfea*. Available at: https://enterfea.com/stress-singularity-an-honest-discussion/

[7] *Getting started with Abaqus (V6.6)*. Available at: https://classes.engineering.wustl.edu/2009/spring/mase5513/abaqus/docs/v6.6/books/gsa/default.htm?startat=ch04s04.html.

[8] Dion *et al.* (1969) *Solving timoshenko beam equation for cantilever beam*, *Engineering Stack Exchange*. Available at: https://engineering.stackexchange.com/questions/48965/solving-timoshenko-beam-equation-for-cantilever-beam

[9] *Bearing pressure* (2022) *Wikipedia*. Wikimedia Foundation. Available at: https://en.m.wikipedia.org/wiki/Bearing_pressure

PART B: Theory of FEA

Table 2 shows the relevant values needed for the solutions to question 2, 3, and 4:

Table 2: Relevant properties for stiffness matrix calculation.

Property	Value
Young's Modulus	215 GPa
Poisson's Ratio	0.33
Node 1 coordinates	(3.72, -0.82)
Node 2 coordinates	(2.55, -0.27)
Node 3 coordinates	(2.57, -1.70)
f1x	115.4 MN/m
f1y	158.5 MN/m

1. a) Number of elements: 69
   b) Number of nodes: 48
   c) Degrees-of-freedom: 96

2. The stiffness matrix of a continuum element (***K***) is given by equation 7.

$$\boldsymbol{K} = \iiint_V \boldsymbol{B}^T(\boldsymbol{r})\boldsymbol{D}\boldsymbol{B}(\boldsymbol{r})\, dV(\boldsymbol{r}) \tag{7}$$

where $\boldsymbol{K}$ is the stiffness matrix, $\boldsymbol{B}(\boldsymbol{r})$ is the derivative of the shape function that converts nodal displacements into strain at any point $\boldsymbol{r}$ within the element**,** $\boldsymbol{D}$ is a material stiffness matrix for an isotropic material

Equation 8 shows an expansion of the matrix $\boldsymbol{D}^{(3D)}$ which is a three-dimensional material property matrix:

$$\boldsymbol{D}^{(3D)} = \frac{E}{(1+\nu)(1-2\nu)} \begin{pmatrix} 1-\nu & \nu & 0 & 0 & 0 & 0 \\ \nu & 1-\nu & \nu & 0 & 0 & 0 \\ \nu & \nu & 1-\nu & 0 & 0 & 0 \\ 0 & 0 & 0 & \frac{1}{2}-\nu & 0 & 0 \\ 0 & 0 & 0 & 0 & \frac{1}{2}-\nu & 0 \\ 0 & 0 & 0 & 0 & 0 & \frac{1}{2}-\nu \end{pmatrix} \text{GPa} \tag{8}$$

where, E is the Young's Modulus (GPa) and ν is the Poisson's ratio.

Equation 9 shows an expansion of the matrix $\boldsymbol{D}^{(2D)}$ which is a two-dimensional material property matrix that includes information about the nature of element such as plane strain:

$$\boldsymbol{D}^{(2D)} = \frac{E}{(1+\nu)(1-2\nu)} \begin{pmatrix} 1-\nu & \nu & 0 \\ \nu & 1-\nu & 0 \\ 0 & 0 & \frac{1}{2}-\nu \end{pmatrix} \text{GPa} \tag{9}$$

Given that the domain consists of Constant Strain Triangles (CST), equation 10 expands matrix $\boldsymbol{B}$**:**

$$\boldsymbol{B} = \frac{1}{2\Delta} \begin{pmatrix} y_2-y_3 & 0 & y_3-y_1 & 0 & y_1-y_2 & 0 \\ 0 & x_3-x_2 & 0 & x_1-x_3 & 0 & x_2-x_1 \\ x_3-x_2 & y_2-y_3 & x_1-x_3 & y_3-y_1 & x_2-x_1 & y_1-y_2 \end{pmatrix} \text{m} \tag{10}$$

where, x_n is the x-coordinate of the nth element node, y_n is the y-coordinate of the nth element node, and Δ is the area of the CST.

Equation 11 shows the calculation of the CST area, using the nodal coordinates in Table 2, it gives a value of 0.8393 m^2

$$\Delta = \frac{1}{2}[(x_2y_3 - x_3y_2) + (x_3y_1 - x_1y_3) + (x_1y_2 - x_2y_1)] \tag{11}$$

Lastly, since the strain is independent of the point $\boldsymbol{r}$ and the thickness of CST is 1, therefore equation 12 calculates the last part of the integral:

$$\boldsymbol{K} = \iiint_V dV\,(\boldsymbol{r}) = \Delta \tag{12}$$

The stiffness matrix in equation 6 is simplified and shown in equation 13:

$$\boldsymbol{K} = \Delta \boldsymbol{B^T D B} \tag{13}$$

$$\boldsymbol{K} = 0.8393 \cdot 10^{11} \begin{pmatrix} 0.85 & 0 & -0.01 \\ 0 & -0.01 & 0.85 \\ -0.52 & 0 & 0.70 \\ 0 & 0.70 & -0.52 \\ -0.33 & 0 & -0.70 \\ 0 & -0.70 & -0.33 \end{pmatrix} \begin{pmatrix} 2.57 & 1.26 & 0 \\ 1.26 & 2.57 & 0 \\ 0 & 0 & 0.65 \end{pmatrix} \begin{pmatrix} 0.85 & 0 & -0.52 & 0 & -0.33 & 0 \\ 0 & -0.01 & 0 & 0.70 & 0 & -0.70 \\ -0.01 & 0.85 & 0.70 & -0.52 & -0.70 & -0.33 \end{pmatrix}$$

$$\boldsymbol{K} = 10^{11} \begin{pmatrix} 1.56 & -0.01 & -0.96 & 0.6373 & -0.60 & -0.63 \\ -0.01 & 0.40 & 0.33 & -0.2532 & -0.32 & -0.14 \\ -0.96 & 0.33 & 0.86 & -0.5926 & 0.10 & 0.26 \\ 0.64 & -0.25 & -0.59 & 1.22 & -0.04 & -0.96 \\ -0.60 & -0.32 & 0.10 & -0.04 & 0.50 & 0.37 \\ -0.63 & -0.14 & 0.26 & -0.96 & 0.37 & 1.11 \end{pmatrix} \text{N/m}$$

3. Equation 14 relates the externally applied forces on the nodes to the nodal displacements:

$$\boldsymbol{f} = \boldsymbol{K u} \tag{14}$$

where, $\boldsymbol{f}$ is the force matrix and $\boldsymbol{u}$ is the nodal displacement matrix.

Using the given force in Table 2 and the calculated stiffness matrix in equation 13, equation 14 is expanded in equation 15, node 2 and 3 movement are restrained in the x and y directions

$$10^6 \cdot \begin{pmatrix} 115.4 \\ 158.5 \\ f_{2x} \\ f_{2y} \\ f_{3x} \\ f_{3y} \end{pmatrix} = 10^{11} \cdot \begin{pmatrix} 1.56 & -0.01 & -0.96 & 0.6373 & -0.60 & -0.63 \\ -0.01 & 0.40 & 0.33 & -0.2532 & -0.32 & -0.14 \\ -0.96 & 0.33 & 0.86 & -0.5926 & 0.10 & 0.26 \\ 0.64 & -0.25 & -0.59 & 1.22 & -0.04 & -0.96 \\ -0.60 & -0.32 & 0.10 & -0.04 & 0.50 & 0.37 \\ -0.63 & -0.14 & 0.26 & -0.96 & 0.37 & 1.11 \end{pmatrix} \begin{pmatrix} u_{1x} \\ u_{1y} \\ 0 \\ 0 \\ 0 \\ 0 \end{pmatrix} \tag{15}$$

Before calculating values for the force matrix, x and y displacements of node 1 need to be found. Equation 16 shows the matrix setup to calculate u_{1x} and u_{1y}.

$$10^6 \cdot \begin{pmatrix} 115.4 \\ 158.5 \end{pmatrix} = 10^{11} \cdot \begin{pmatrix} 1.56 & -0.01 \\ -0.01 & 0.40 \end{pmatrix} \begin{pmatrix} u_{1x} \\ u_{1y} \end{pmatrix} \tag{16}$$

$$\begin{pmatrix} u_{1x} \\ u_{1y} \end{pmatrix} = 10^{-5} \cdot \left[\begin{pmatrix} 1.56 & -0.01 \\ -0.01 & 0.40 \end{pmatrix} \right]^{-1} \begin{pmatrix} 115.4 \\ 158.5 \end{pmatrix}$$

$$\begin{pmatrix} u_{1x} \\ u_{1y} \end{pmatrix} = 10^{-3} \cdot \begin{pmatrix} 0.765 \\ 3.98 \end{pmatrix} m$$

Equation 14 can now be calculated to give the force on each node in the x and y directions:

$$\boldsymbol{f} = 10^8 \cdot \begin{pmatrix} 1.1638 \\ 1.5732 \\ 0.5784 \\ -0.5202 \\ -1.7422 \\ -1.0530 \end{pmatrix} N$$

Equation 17 calculates the magnitude of the node 2 reaction force:

$$F_2 = \sqrt{f_{2x}^2 + f_{2y}^2} \tag{17}$$

$$\therefore \boldsymbol{F_2 = 77.79\ \text{MN}}$$

4. To find the natural frequencies of vibration, an equation of motion for a dynamic model has to be set up, as seen in equation 18, the model must also contain no external forces therefore letting it to vibrate freely.

$$\boldsymbol{M\ddot{u}}(t) + \boldsymbol{C\dot{u}}(t) + \boldsymbol{Ku}(t) = \boldsymbol{0} \tag{18}$$

where, $\boldsymbol{M}$ is the mass matrix, $\boldsymbol{C}$ is the damping matrix, $\boldsymbol{K}$ is the stiffness matrix, $\boldsymbol{u}(t)$ is the nodal displacement matrix, $\dot{\boldsymbol{u}}(t)$ is the nodal velocity matrix (1st derivative of $\boldsymbol{u}(t)$), and $\ddot{\boldsymbol{u}}(t)$ is the nodal acceleration matrix (2nd derivative of $\boldsymbol{u}(t)$).

The mass matrix $\boldsymbol{M}$ can be found since the distribution of the mass in the domain is known. The damping matrix $\boldsymbol{C}$ is equal to zero since material damping is negligible. The stiffness $\boldsymbol{K}$ can be calculated using equation 12. Since the system is linear, all displacements are assumed to be harmonic (sinusoidal) in the steady-state solution, equation 19 and 20 express equations for nodal displacement and acceleration, respectively.

$$\boldsymbol{u}(t) = \begin{pmatrix} \tilde{u}_1 \\ \tilde{u}_2 \\ \vdots \end{pmatrix} e^{-j\omega t} = \tilde{\boldsymbol{u}} e^{-j\omega t} \tag{19}$$

$$\ddot{\boldsymbol{u}}(t) = -\omega^2 \tilde{\boldsymbol{u}} e^{-j\omega t} \tag{20}$$

Substituting the equations for nodal displacement and acceleration into the equation of motion causes the $e^{-j\omega t}$ to cancel, therefore:

$$-\omega^2 \boldsymbol{M}\tilde{\boldsymbol{u}} + \boldsymbol{K}\tilde{\boldsymbol{u}} = (-\omega^2 \boldsymbol{M} + \boldsymbol{K})\tilde{\boldsymbol{u}} = \boldsymbol{0} \tag{21}$$

To solve for the natural frequencies, the expressions need to arrive to an eigenvalue situation. The determinant of $(-\omega^2 \boldsymbol{M} + \boldsymbol{K})$ is set to zero, hence:

$$|\boldsymbol{K} - \omega^2 \boldsymbol{M}| = 0 \tag{22}$$

Equation 21 is a matrix expression that generates a polynomial equation where its order is equal to the degrees of freedom the system has, which is therefore then solved to obtain the natural frequencies of vibration.

REFERENCES

1. H. Coules, 2022, MENG33111 Finite Element Analysis, FE 4 – Continuum elements I, University of Bristol

PART C: Failure of Materials

Question 1

Table 3: Material properties of structural component and relevant values used for calculations in Question 1

Property	Value
Yield stress	400 MPa
Elastic modulus	70 GPa
Poisson's Ratio	0.3
Fracture toughness	20 MPa$\sqrt{m}$
Additional stress 'P'	-400 to 400 MPa
Additional stress direction	30°
Crack length	5mm
Strain in x-direction	-0.0015
Strain in y-direction	0.0029

Question 1a

The smallest number of strain measurements required to determine σ_x and σ_y is two, assuming the strain gauge direction is not parallel during the strain measurements.

Question 1b

The structural component is in a state of plane stress since the normal stresses act in only the x and y dimensions. To calculate the applied stresses σ_x and σ_y Hooke's law is applied in equation 23 and 24 as the material is homogenous and behaves in a linear elastic manner:

$$\varepsilon_x = \frac{\sigma_x}{E} - \frac{\nu\sigma_y}{E} - \frac{\nu\sigma_z}{E} \tag{23}$$

$$\varepsilon_y = \frac{\sigma_y}{E} - \frac{\nu\sigma_x}{E} - \frac{\nu\sigma_z}{E} \tag{24}$$

where, ε_n is the strain acting in the n direction, σ_n is the normal stress in the n direction, ν is the Poisson's ratio, and E is the Young's modulus.

Hooke's law is then rearranged and simplified to calculate the applied stresses in the x and y directions, stress in the z direction is neglected, given by equation 25 and 26:

$$\sigma_x = \frac{E}{1-\nu^2}\left(\varepsilon_x + \nu\varepsilon_y\right) \tag{25}$$

$$\sigma_y = \frac{E}{1-\nu^2}\left(\nu\varepsilon_x + \varepsilon_y\right) \tag{26}$$

The provided MATLAB strain function uses strain gauge orientations of θ = 0° and 90° which result in strain values of ε_x = -0.0015 and ε_y = 0.0029 respectively. The strain measurements and values in Table 1 result in the following stress values for the x and y directions:

$$\sigma_x = \text{-}48.46 \text{ MPa}$$
$$\sigma_y = 188.46 \text{ MPa}$$

Question 1c

This part of the question provides an analysis of the structural component's possible failure mechanisms in relation to the applied stress σ_p. Based on the information provided about the component and its crack, two failure mechanisms are considered: yielding and brittle fracture. Before considering additional stress, the initial stress tensor requires the shear stress value due to σ_x and σ_y. Equation 27 and 28 uses the MATLAB function at 45° strain gauge orientation to determine shear stress.

$$\varepsilon_{xy} = \varepsilon_{45} - \frac{\varepsilon_0 + \varepsilon_{90}}{2} \tag{27}$$

where, ε_n is the strain at n° strain gauge orientation.

$$\sigma_{xy} = \frac{E \cdot \varepsilon_{xy}}{2(1+\upsilon)} \tag{28}$$

Failure mechanism: Ductile failure

Considering yielding of the component first, both Von Mises and Tresca failure criteria are applied to the problem. Given that there is an additional applied stress σ_p at θ_p, being 30° measured from the x-axis, the coordinate system must be rotated. The calculated shear stress value in Equation 28 is negligible and hence is used as zero. Equation 29 shows the initial stress tensor prior to rotation ($\boldsymbol{\sigma_i}$):

$$\boldsymbol{\sigma_i} = \begin{pmatrix} \sigma_x & 0 \\ 0 & \sigma_y \end{pmatrix} = \begin{pmatrix} -48.46 & 0 \\ 0 & 188.46 \end{pmatrix} \tag{29}$$

Equation 30 gives the rotation matrix ($\boldsymbol{\sigma_r}$):

$$\boldsymbol{\sigma_r} = \begin{pmatrix} cos(30) & sin(30) \\ -sin(30) & cos(30) \end{pmatrix} \tag{30}$$

Equation 31 shows the initial stress tensor rotated using the rotation matrix ($\boldsymbol{\sigma}$):

$$\boldsymbol{\sigma} = \boldsymbol{\sigma_r} \cdot \boldsymbol{\sigma_i} \cdot \boldsymbol{\sigma_r^T} = \begin{pmatrix} cos(30) & sin(30) \\ -sin(30) & cos(30) \end{pmatrix} \begin{pmatrix} -48.46 & 0 \\ 0 & 188.46 \end{pmatrix} \begin{pmatrix} cos(30) & -sin(30) \\ sin(30) & cos(30) \end{pmatrix} \tag{31}$$

$$\therefore \boldsymbol{\sigma} = \boldsymbol{\sigma_r} \cdot \boldsymbol{\sigma_i} \cdot \boldsymbol{\sigma_r^T} = \begin{pmatrix} 10.62 & 102.68 \\ 102.68 & 129.18 \end{pmatrix}$$

Finally, equation 32 shows the stress tensor with the applied stress (σ_{new}):

$$\boldsymbol{\sigma_{new}} = \boldsymbol{\sigma} + \boldsymbol{\sigma_p} = \begin{pmatrix} 10.62 & 102.68 \\ 102.68 & 129.18 \end{pmatrix} + \begin{pmatrix} \sigma_p & 0 \\ 0 & 0 \end{pmatrix} = \begin{pmatrix} 10.62 + \sigma_p & 102.68 \\ 102.68 & 129.18 \end{pmatrix} \tag{32}$$

The principles stresses are then found using equation 33 for both Von Mises and Tresca equations, using the eigenvalues of the new stress tensor. They are functions of additional stress σ_p:

$$\sigma_{1,2} = \frac{\sigma_{11} + \sigma_{22}}{2} \pm \sqrt{\left(\frac{\sigma_{11} - \sigma_{22}}{2}\right)^2 + \sigma_{12}^2} \tag{33}$$

Von Mises and Tresca stress are then therefore found using equations 34 and 35, respectively:

$$\sigma_{VM} = \sqrt{\frac{(\sigma_1 - \sigma_2)^2 + \sigma_1^2 + \sigma_2^2}{2}} \tag{34}$$

$$\sigma_T = max(|\sigma_1 - \sigma_2|, |\sigma_1|, |\sigma_2|) \tag{35}$$

The safety factors of Von Mises and Tresca stress are given by equation 36 and 37, respectively:

$$SF_{VM} = \frac{\sigma_Y}{\sigma_{VM}} \tag{36}$$

$$SF_T = \frac{\sigma_Y}{\sigma_T} \tag{37}$$

where, σ_Y is yield stress and is given in Table 3.

Figure 4 displays the range of additional stress σ_p varying with each failure criteria's equivalent stress and safety factor. Table 4 summarizes the range of values that do not cause yield to the structural component and a safety factor for the Von Mises and Tresca criteria. The Tresca failure criterion is more conservative than Von Mises as it predicts a narrower elastic region and provides a safer upper limit for the additional stress. In a scenario where it is crucial that a component does not fail, the Tresca criterion is normally used and hence is used in this scenario.

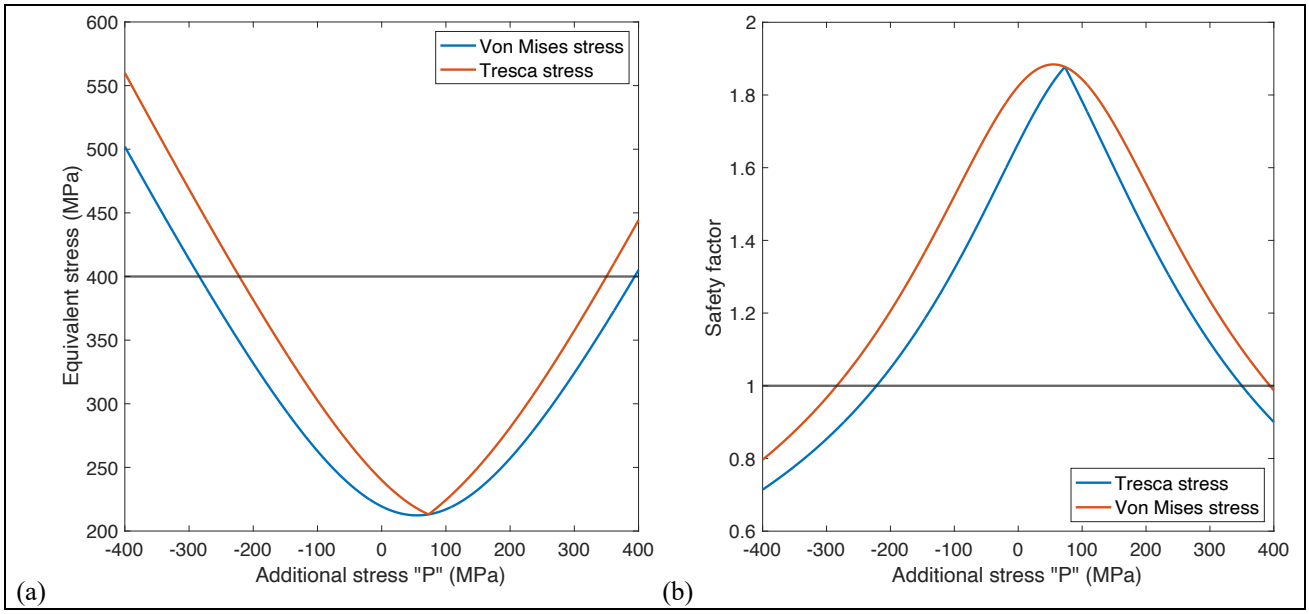

Fig. 4 Displays how the additional stress σ_p varies with (a) equivalent stress and (b) safety factor for Von Mises and Tresca failure criteria.

Table 4: Range of additional stress σ_p values for the two failure criteria

Failure criteria	Lower bound for stress (σ_p)	Upper bound for stress (σ_p)	Safety factor
Von Mises	-284 MPa	394 MPa	1.88
Tresca	-222 MPa	350 MPa	1.88

Failure mechanism: Brittle failure

Considering brittle failure, the central crack and its effect on the structural component is analyzed. Given that the crack is central on the component, the plate geometry correction Y is 1. Since the load is normal to the crack orientation, tensile stress is perpendicular to the crack since it is in mode one loading. As a result, the stress intensity factor is given by equation 38:

$$K_I = Y\sigma_t\sqrt{\pi a} \tag{38}$$

where, K_I is the stress intensity factor, Y is the plate geometry correction, σ_t is the tensile stress perpendicular to the crack, and a is the crack length divided by two.

The structural component will fracture when the stress intensity factor K_I equals the fracture toughness K_{IC} provided. The brittle fracture safety factor is given by equation 39:

$$SF_K = \frac{K_{IC}}{K_I} \tag{39}$$

This failure mechanism uses the values of additional stress σ_p, crack orientation θ, and stress intensity factor K_{IC} for determining fracture in the structural component. The stress has a range of $|\sigma_p| \leq 400$ MPa and the crack orientation varies from 0° to 180° since the crack orientation from 180° to 360° would be the same.

Linear elastic fracture mechanics (LEFM) is applied to the component during its fatigue process. Equation 40 presents the LEFM validity equation, if a is greater than the latter part of the equation, the crack length is 'valid' meaning that the plastic zone is negligible.

$$a \geq \frac{4}{\pi}\left(\frac{K_I}{\sigma_y}\right)^2 \tag{40}$$

Figure 5(a) shows how the stress intensity factor varies with additional stress σ_p and orientation of the crack, it also shows the stress intensity value that cannot be used (green region) having a value of $K_I = 20$ and the values that can be used (white region). Figure 5(b) uses the stress intensity values from Figure 5(a) and equation 40 to display the crack length values that are validated by LEFM and those that are not. The crack length values that are in blue (not cyan) are validated by LEFM, the ones that are not are validated using LEFM, are validated using elastic plastic fracture mechanics (EPFM).

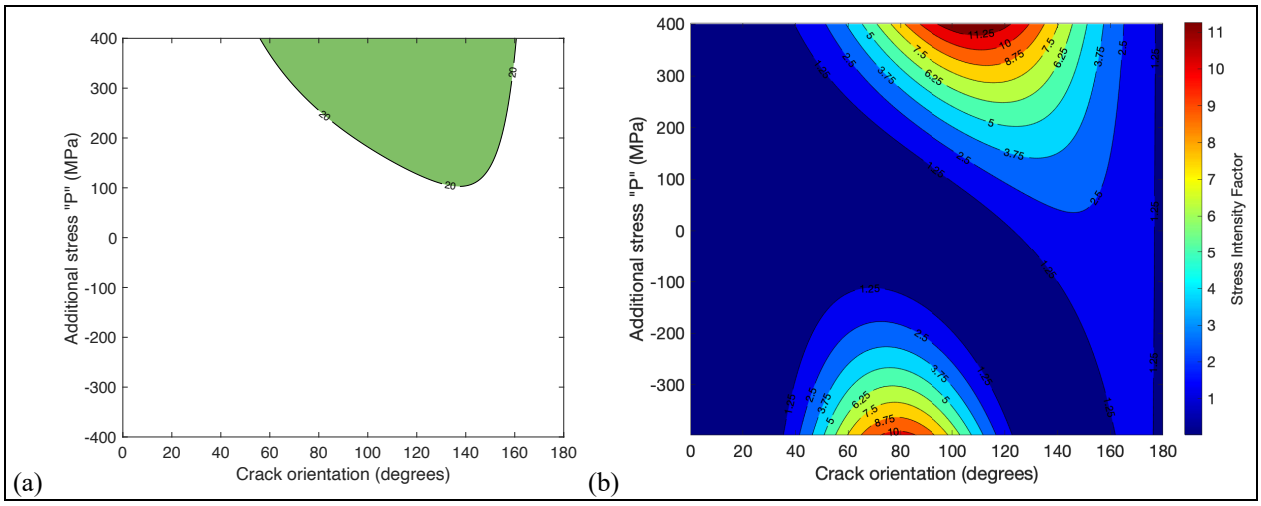

Fig. 5 Displays how (a) stress intensity factor varies with the crack orientation and additional stress (LEFM), also displays the (b) valid and invalid crack length values due to the LEFM validity.

The crack length values that need to be validated using EPFM using 'Irwin correction' is displayed in equation 41:

$$K_{eff} = \frac{\sigma_t\sqrt{\pi a}}{\sqrt{1-\frac{1}{2}\left(\frac{\sigma_t}{\sigma_y}\right)^2}} \tag{41}$$

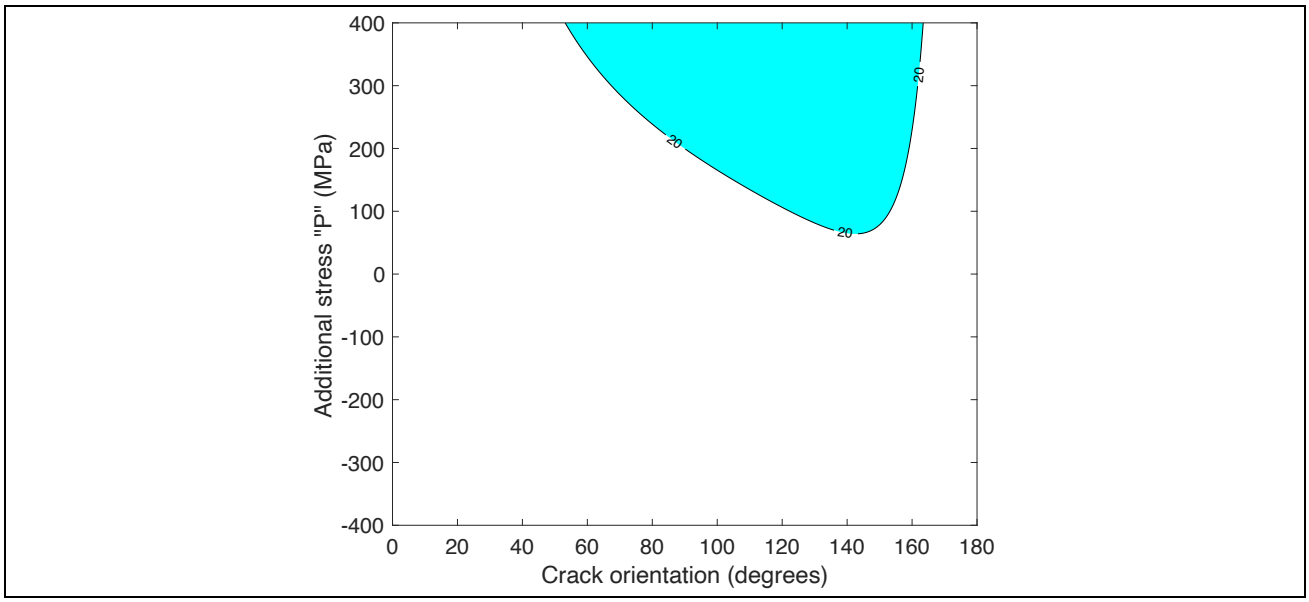

Fig. 6 Displays how the stress intensity factor varies with the crack orientation and additional stress after EPFM.

Therefore, the plot in Figure 6 displays how the stress intensity K_I validated by EPFM varies with crack orientation and the additional stress σ_p

In summary, the brittle fracture failure mechanism using the analysis explained above provides a value for the most dangerous crack orientation. By reading off the lowest additional stress value at stress intensity K_I = 20 from figure 6, the most dangerous crack orientation is 30° + 143° = **173**°. Table 5 provides the safe range of additional stress σ_p values that is safe for the structural integrity of the component. The lower limit is the lower bound of the Tresca criterion and the upper limit is the additional stress value at 20 stress intensity after EPFM read from the plot in Figure 6.

Table 5: Safe range of additional stress values

	Lower bound	Upper bound
Additional stress (σ_p)	-222 MPa	64 MPa

Question 2

Table 6: Relevant values used for calculations in Question 2

Property	**Value**
Pipe outer diameter	200 mm
Pipe wall thickness	10 mm
Pipe internal pressure	0 to 40 MPa
Fracture toughness	90 MPa$\sqrt{m}$
Paris' law constant C	10^{-12}
Paris' law constant m	4
Crack length	5 mm
Strain in x-direction	-0.0015
Strain in y-direction	0.0029

Probability of detection vs crack length

The given problem at hand is to determine how the pipe's probability of failure depends on the interval between pipe inspections and to determine the inspection interval corresponding to a probability of failure equal to 0.01. Initially, to understand how the 'probability of detecting a crack' changes when its crack length varies, Figure 7(b) plots the probability of detection with crack length (2a) to determine this relationship. Figure 7(a) plots the probability of not detecting the crack varying with crack length 0.6mm to 20mm. An arbitrary value for inital crack radius (a_i = 0.3mm) is chosen from values that are most commonly used for steels [2]. The final crack radius (a_f = 10mm) is chosen as at 10mm the crack in the pipe would have the same length as the thickness of the pipe resulting in complete failure.

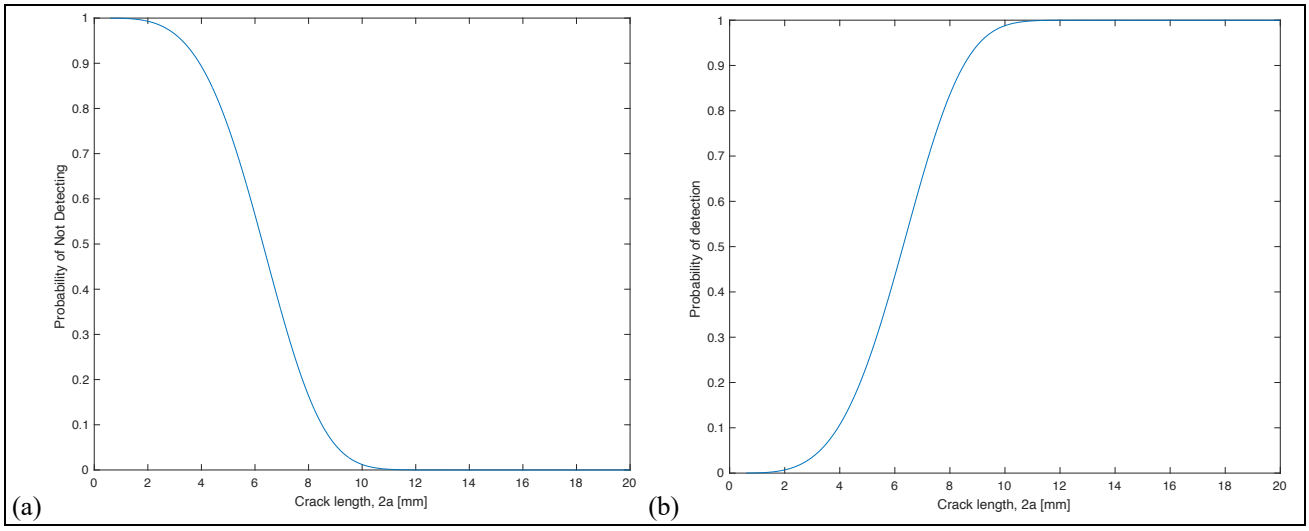

Fig. 7 Displays the (a) probability of not detecting a crack with length 2a and (b) probability of detecting a crack with length 2a.

Equation 42 shows the probability of not detecting a crack at length 2a or higher for a single inspection:

$$P(pod') = 1 - P(pod) \tag{42}$$

where, $P(pod')$ is the probability that the crack is not detected, $P(pod)$ is the probability of detecting a crack of radius a.

Failure mechanisms

Next, the failure mechanism that occurs quicker needs to be determined: leakage or fracture of the pipe. Due to mode 1 loading of the pipe, the stress is normal to the crack is responsible for increasing the length of the crack in the pipe. Therefore, equation 43 defines the axial stress of the component:

$$\sigma_{axial} = \frac{pr}{2t} \tag{43}$$

where, p is the working pressure of the pipe, r is the outer radius of the pipe, and t is the thickness of the pipe.

For the failure mechanism of fracture before leakage the stress intensity factor K_I when a = 10 mm would need to be greater than fracture toughness. Equation 44 and 45 are used for the stress intensity factor.

$$K_I = K_{IC} = Y\sigma_{max}\sqrt{\pi a_f} \tag{44}$$

where, K_{IC} fracture toughness from Table 6, Y is the geometry correction factor for the semi-circular crack, σ_{max} is the maximum stress from cyclic loading

$$Y = 0.728 + 0.373\left(\frac{a}{t}\right)^2 - 0.029\left(\frac{a}{t}\right)^4, a \leq t \tag{45}$$

where, t is the wall thickness.

Assuming that the axial stress can be used as the design stress, the stress intensity factors for working pressures of 40 MPa and 80 MPa are 38 MPa$\sqrt{m}$ and 76 MPa$\sqrt{m}$ respectively. In conclusion, this implies that the pipe fails by leakage.

Number of cycles until failure

Equation 46 is derived from Paris Law, which calculates the number of cycles it takes to grow a crack from initial to final length:

$$N = \int_{a_i}^{a_f} \frac{1}{C\left(Y\Delta\sigma\sqrt{\pi a}\right)^m} \tag{46}$$

where, N is the number of cycles until failure, a_i is the initial crack radius, a_f is the crack radius at failure, C and m are constants given in Table 6, Y is the geometry correction factor, and $\Delta\sigma$ is the difference in the minimum and maximum stress during cyclic loading.

$\Delta\sigma$ is equal to the axial stress corresponding to the maximum working pressure since the minimum working pressure is zero. Equation 46 results in 696,862 cycles for crack radius from 0.3mm to 10mm. Equation 47 is used to determine crack growth rate $\left(\frac{da}{dN}\right)$ during each cyclic loading:

$$\frac{da}{dN} = C\left(Y\Delta\sigma\sqrt{\pi a}\right)^m \tag{47}$$

Equation 48 is used to loop the Paris Law growth from crack radius 0.3mm to 10mm:

$$a_n + \frac{da_n}{dN} = a_{n+1} \tag{48}$$

Figure 8 shows how crack length 2a increases as the number of cycles increases.

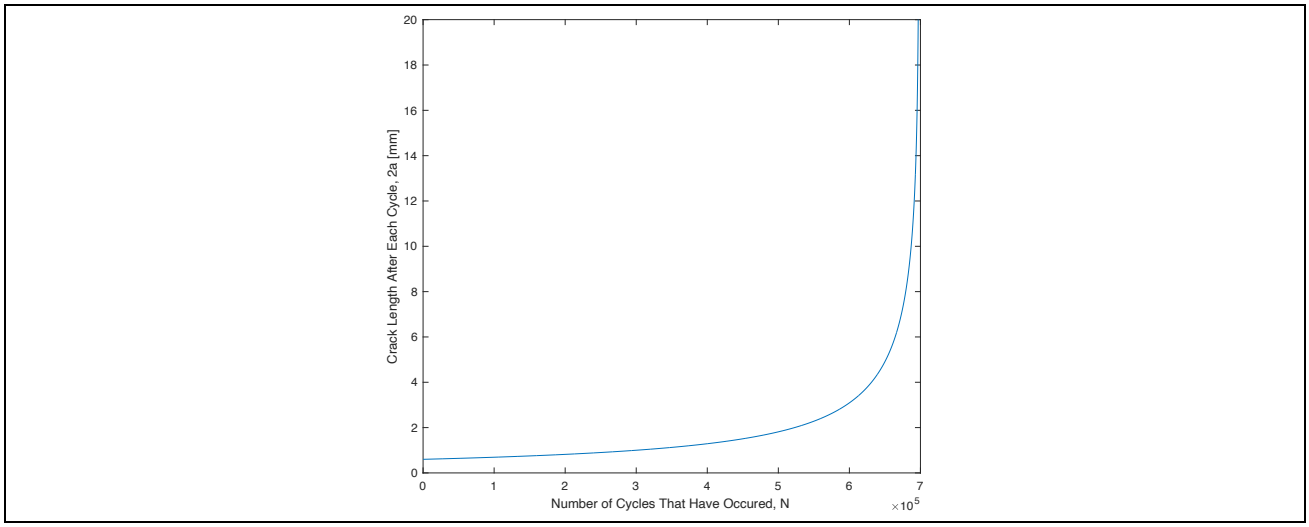

Fig. 8 Number of cycles until failure against crack length.

Probability of failure

The probability of a crack not being detected depends on the crack length in that specific instance, presented in Figure 7(b). The following analysis will consider the probability of not detecting a crack per inspection until the pipe fails or the final inspection is reached. Equation 49 is used for the remaining analysis:

$$\frac{da}{dN} = C\left(Y\Delta\sigma\sqrt{\pi a}\right)^m \tag{49}$$

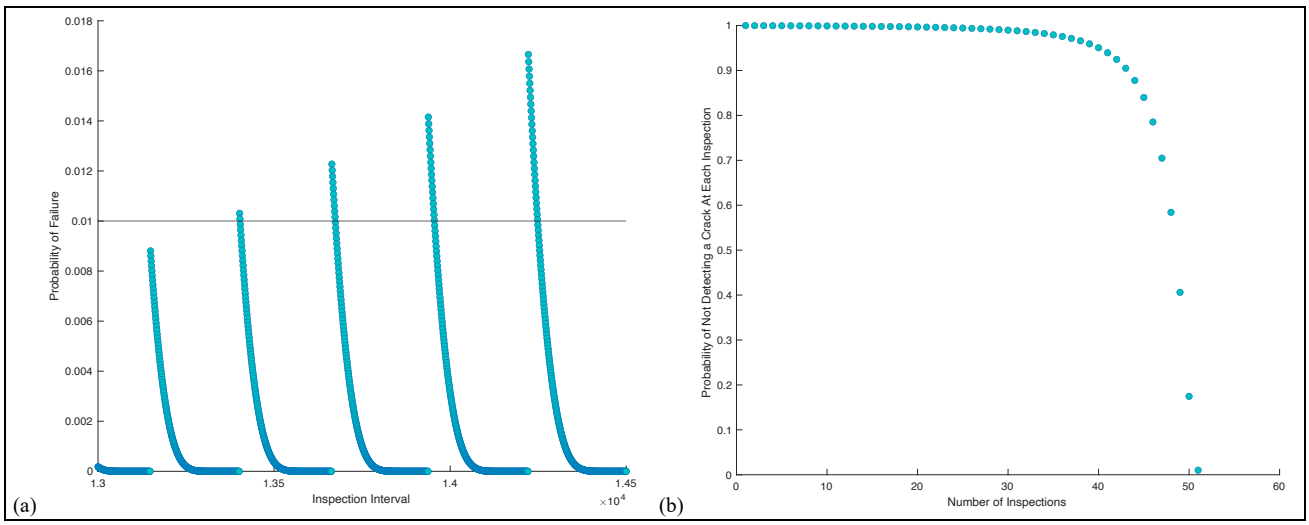

Fig. 9 (a) Probability of failure against inspection intervals and (b) Probability of not detecting a crack at every inspection for a specific interval.

Question 2a

Probability of failure is the probability at which a crack is undetected after all inspections until the pipe fails. The number of inspections depends on the interval between inspections implying that the probability of failure depends on the interval between the inspections carried out.

Question 2b

Figure 9(a) shows that the probability of failure equal to 0.01 is first detected between intervals **13,403 and 13,404.** Figure 9(b) shows that at the 51st inspection, the probability of not detecting a crack at that inspection is zero.

REFERENCES

[1] Harry Coules & Alexander Velichko, 07/11/2022, MENG 30011 Applied Solid Mechanics, AY 2022/23 coursework assessment, University of Bristol.

[2] Author links open overlay panelDieterRadajDr-Ing habil and habil, D.R.D.-I. (2014) *Fracture Mechanics Approach for assessment of fatigue strength of seam welded joints*, *Design and Analysis of Fatigue Resistant Welded Structures*. Woodhead Publishing. Available at: https://www.sciencedirect.com/science/article/pii/B9781855730045500131